

Anthropogenic CO₂ emissions from a megacity in the Yangtze River Delta of China

Cheng Hu^{1,2,3}  · Shoudong Liu^{1,2} · Yongwei Wang^{1,2} · Mi Zhang^{1,2} · Wei Xiao^{1,2} · Wei Wang^{1,2} · Jiaping Xu^{1,4}

Received: 3 January 2018 / Accepted: 15 May 2018 / Published online: 3 June 2018

© Springer-Verlag GmbH Germany, part of Springer Nature 2018

Abstract

Anthropogenic CO₂ emissions from cities represent a major source contributing to the global atmospheric CO₂ burden. Here, we examined the enhancement of atmospheric CO₂ mixing ratios by anthropogenic emissions within the Yangtze River Delta (YRD), China, one of the world's most densely populated regions (population greater than 150 million). Tower measurements of CO₂ mixing ratios were conducted from March 2013 to August 2015 and were combined with numerical source footprint modeling to help constrain the anthropogenic CO₂ emissions. We simulated the CO₂ enhancements (i.e., fluctuations superimposed on background values) for winter season (December, January, and February). Overall, we observed mean diurnal variation of CO₂ enhancement of 23.5~49.7 $\mu\text{mol mol}^{-1}$, 21.4~52.4 $\mu\text{mol mol}^{-1}$, 28.1~55.4 $\mu\text{mol mol}^{-1}$, and 29.5~42.4 $\mu\text{mol mol}^{-1}$ in spring, summer, autumn, and winter, respectively. These enhancements were much larger than previously reported values for other countries. The diurnal CO₂ enhancements reported here showed strong similarity for all 3 years of the study. Results from source footprint modeling indicated that our tower observations adequately represent emissions from the broader YRD area. Here, the east of Anhui and the west of Jiangsu province contributed significantly more to the anthropogenic CO₂ enhancement compared to the other sectors of YRD. The average anthropogenic CO₂ emission in 2014 was 0.162 (± 0.005) mg m⁻² s⁻¹ and was 7 \pm 3% higher than 2010 for the YRD. Overall, our emission estimates were significantly smaller (9.5%) than those estimated (0.179 mg m⁻² s⁻¹) from the EDGAR emission database.

Keywords Anthropogenic CO₂ emissions · Megacity · WRF-STILT model · Tall tower observations · Yangtze River Delta · China

Responsible editor: Gerhard Lammel

- ✉ Cheng Hu
huxxx991@umn.edu
- ✉ Shoudong Liu
lsd@nust.edu.cn

¹ Yale-NUIST Center on Atmospheric Environment, International Joint Laboratory on Climate and Environment Change (ILCEC), Nanjing University of Information, Science & Technology, Nanjing 210044, China

² Key Laboratory of Meteorological Disaster, Ministry of Education (KLME), Collaborative Innovation Center on Forecast and Evaluation of Meteorological Disasters (CIC-FEMD), Nanjing University of Information, Science & Technology, Nanjing 210044, China

³ Department of Soil, Water, and Climate, University of Minnesota-Twin Cities, Soil Science Room 331, 1991 Upper Buford Circle, St. Paul, MN 55108, USA

⁴ Key Laboratory of Transportation Meteorology, China Meteorological Administration, Nanjing 210009, Jiangsu, China

Introduction

Anthropogenic carbon dioxide (CO₂) emissions play an important role in the global carbon budget and the greenhouse gas radiative budget (McKain et al. 2012). Regions with high population and industry density are hotspots for CO₂ emissions. Interestingly, cities account for 70% of the total anthropogenic emissions, but account for only 2% of the global land surface (Satterthwaite 2008; Canadell et al. 2010). Emissions from urban ecosystems are directly related to fuel consumption from electricity generation, industry, and transportation. Reports from the United Nations predict that the population living in cities will increase from 3.4 billion to 6.3 billion by the year 2050 (Rosenzweig et al. 2010). This increase imposes a potentially large burden on policy makers to help control CO₂ emissions and to develop mitigation strategies. There is an important need therefore to better quantify anthropogenic CO₂ emissions from major urban areas and to improve our understanding of the patterns and controls on CO₂ emissions (Xu et al. 2017; Sun et al. 2017). Here, we examine CO₂

emissions from the Yangtze River Delta of China where the total population is approximately 150 million.

Both “top-down” and “bottom-up” methods have been applied in quantifying urban CO₂ emissions. Bottom-up methods such as the IPCC (Inter-governmental Panel on Climate Change) inventory method use activity data and emission factors to calculate emissions from each category and section to determine the total CO₂ budget at the local to regional scale (IPCC 2013). The default emission factors for different fossil fuel categories have been established and applied globally. However, relatively large biases still exist for a number of source categories. For example for the same fossil fuel type, the emission factors can vary widely depending on country or even region within the same country (Rypdal and Winiwarter 2001; Zhao et al. 2012; Liu et al. 2015). Liu et al. (2015) found that emission factors in China were much larger than default values based on experiments conducted in coal-mining regions. Such discrepancies in activity data and emission factors can lead to ~ 40% uncertainty at the country or regional scale and as much as 150% at the local scale (Peylin et al. 2013; Wang et al. 2013). Many anthropogenic CO₂ emission maps are based on the IPCC method. To date, they provide the most widely used anthropogenic CO₂ information and are often used for computing inventory statistics and used in model simulations (Peters et al. 2007; Gurney et al. 2009; European Commission 2009). These emission maps are treated as a priori data and need to be evaluated and tuned to improve emission estimates worldwide.

Top-down methods have been used in recent years to retrieve CO₂ emissions at regional scales via remote sensing, atmospheric transport models, and atmospheric CO₂ mixing ratio observations (Mckain et al. 2012; Kort et al. 2012, 2013; Staufer et al. 2016; Sun et al. 2017; Hu et al. 2018). This method is based on the theory that the enhancement in atmospheric concentrations relative to background values can be used to track anthropogenic emissions over megacities (Kort et al. 2013). For its strength in continuous temporal scale and finer spatial scale, atmospheric transport models shown large potential in CO₂ flux retrievals.

Early inverse studies focused on estimating net ecosystem CO₂ flux with anthropogenic emission prescribed as true values (Peters et al. 2007; Gurney et al. 2009; Ogle et al. 2015). Recent studies have applied this inverse method for constraining anthropogenic emissions and have demonstrated reasonably good performance. To date, this methodology has been applied to Paris (Bréon et al. 2015; Staufer et al. 2016), Berlin (Pillai et al. 2016), California’s Bay Area (Kort et al. 2013; Turner et al. 2016), Indianapolis (Turnbull et al. 2015), Salt Lake City (Mckain et al. 2012), and Minneapolis-St.Paul, Minnesota (Hu et al. 2018), while this method has not yet been applied in China for anthropogenic CO₂ retrieval, where urban areas are extremely dense and the economy has rapidly developed. This is especially true for the Yangtze River Delta, which represents

a megacity complex and a population of about 150 million. Indeed, as a human-dominated landscape, the Yangtze River Delta ranks as one of the densest urbanized regions of the world and one of the most developed regions in China (Jiangsu, Zhejiang, Anhui province, and Shanghai municipality). Its area accounts for only 2.2% of China, yet represents 11% of the national population. It accounts for about 18.5% of China’s GDP in 2014. The Nanjing municipality is also the second-largest city in YRD with a population of 8 million. Thus, the YRD is a potential hot spot for anthropogenic CO₂ emissions. Based on IPCC statistics, anthropogenic CO₂ emissions were reported to be $66.49 (\pm 8\%) \times 10^9$ kg in Nanjing and $15.35 (\pm 10\%) \times 10^{11}$ kg for YRD in 2009 (Shen et al. 2014). Xu et al. (2017) used the IPCC methodology and estimated an increase of anthropogenic CO₂ emissions by about 70% since 2009 in response to the rapid increase in GDP for this period. These previous studies are based on “bottom-up” methods and there is an important need to use top-down approaches to help confirm the magnitude of these emissions.

To constrain the anthropogenic CO₂ emissions in YRD, we have conducted atmospheric CO₂ mixing ratio measurements at a height of 34 m over a period of nearly 3 years. We combined these observations with an atmospheric transport model and a priori emission maps to simulate atmospheric CO₂ enhancements and used this information to help constrain the anthropogenic CO₂ emissions. The objectives of this study are to (1) establish the first long-term CO₂ mixing ratio observations in the Yangtze River Delta and analyze its seasonal variations based on WRF-STILT simulations; (2) evaluate if the CO₂ mixing ratio observations are representative of the Yangtze River Delta; and (3) constrain the anthropogenic emissions using a top-down methodology and compare this estimate with the most recent bottom-up estimate from EDGAR42 for the year 2014.

Materials and methodology

Research site

The atmospheric CO₂ mixing ratios were measured on the rooftop of the Meteorology building (34 m) located at the Nanjing University of Information Science and Technology (32° 12' N, 118° 43' E). This measurement site is located 25 km north of Nanjing municipality, China, (Fig. 1). The Nanjing municipality is close to the center of YRD and ranks as the second largest city (population of 8 million). The Yangtze River encompasses Jiangsu, Zhejiang, Anhui province, and Shanghai municipality (Fig. 1).

Our measurements were near continuous from March 2013 to August 2015. Air was measured at a flow rate of 30 mL min⁻¹ and recorded to a data logger at 0.3 Hz. To ensure high accuracy of the CO₂ measurements, the analyzer (model

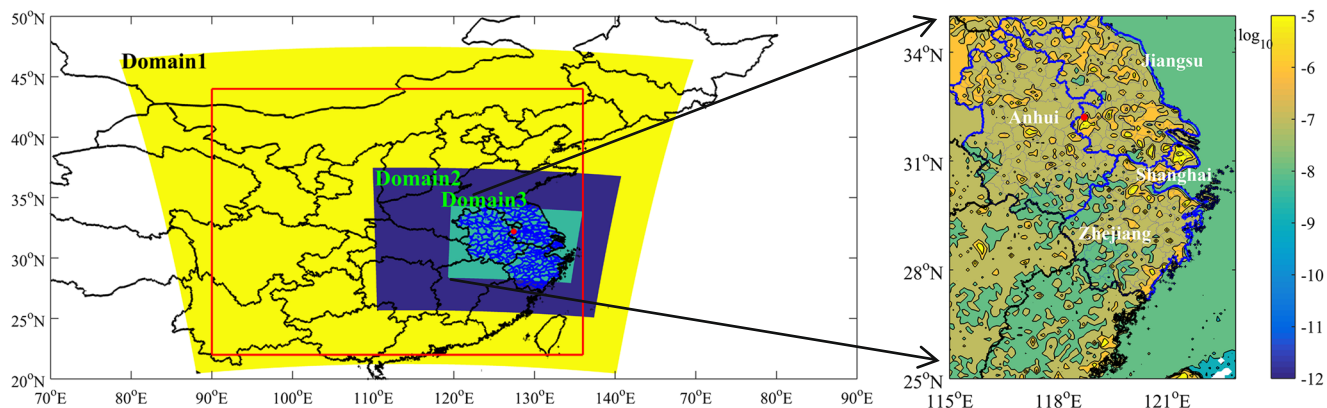


Fig. 1 Study domains for WRF3.5 model, the area in red square is the domain for STILT model, total anthropogenic CO₂ emission map in Yangtze River Delta is displayed on the right (unit mol m⁻² s⁻¹), with red dot denote our observation site location

G1101-i, Picarro, Inc. Sunnyvale, CA) was calibrated every 3 h with standards traceable to the National Oceanic and Atmospheric Administration, Earth System Research Laboratory (NOAA-ESRL). The precision of the hourly averaged CO₂ mixing ratios was typically 0.1 μmol mol⁻¹ (Xu et al. 2017).

CO₂ a priori anthropogenic emissions

IPCC method applied activity data and emission factors to estimate fossil fuel CO₂ emissions; the emission factors are derived from the synthesis of field observations and modeling. As noted above, large uncertainty and bias can exist in both emission factors and activity data and can propagate into the derived CO₂ emissions. The EDGAR (Emission Database for Global Atmospheric Research, version 4.2, 2011, <http://edgar.jrc.ec.europa.eu>) and VULCAN (Gurney et al. 2009) are two popular products and based on the IPCC methodology. They provided to date most excellent distribution at finer spatial scale. For the reason that VULCAN owned hourly scaling factors for each anthropogenic CO₂ flux in all categories while was only available to 2002, EDGAR provided annual mean CO₂ emission for the year of 2010; here, anthropogenic CO₂ emissions from EDGAR and hourly scaling factors from VULCAN will be applied in our study, and we will build our constraint based on these available a priori product and this method was described in greater details below.

EDGAR v4.2 provides 13 anthropogenic emission categories including residential, oil production (refineries) industry, energy industry, road transportation, manufacturing industry combustion, combustion in manufacturing industry, and other anthropogenic categories (i.e., mineral process and solid waste disposal). According to our preliminary analyses, the first 6 categories accounted for 85% of the total anthropogenic CO₂ emissions in YRD. The energy industry, road transportation, and residential and manufacturing industry categories accounted for 43, 22.4, 12.9, and 8.6%, respectively. The latest EDGAR v4.2 only provides emission maps up to the year

2010 and does not directly match our observational period (2013 to 2015). To obtain an a priori emission map for our study period, we assume the spatial distribution of emissions for 2013 to 2015 is consistent with the year 2010 and we have adjusted the total emissions for the study domain based on the CO₂ emissions in 2014 (107.11 Gtons) and 2010 (89.87 Gtons) for China (<http://edgar.jrc.ec.europa.eu>). Therefore, a ratio of 1.18 (107.11/89.87) was applied in order to estimate the emissions for our study period. Anthropogenic emissions from residential, on-road transportation, and combustion in manufacturing industry are shown in Fig. 2. The emission map shown excellent distribution of anthropogenic CO₂ information; two of the largest industrial complexes Nanjing Iron & Steel Group and Chemical Industry Group Co. Ltd. were in 5 km distance with our observation site and were reflected by EDGAR emissions with CO₂ emissions from oil industry 4.4×10^{-5} and 7.3×10^{-5} mol m⁻² s⁻¹ (energy industry 1.1×10^{-4} mol m⁻² s⁻¹) at the same locations.

To simulate the diurnal variation of CO₂ emissions, we derived hourly scaling factors based on the VULCAN database (Gurney et al. 2009) for industry, residential, and road transportation (Hu et al. 2018). This approach accounts for the diurnal variations of different human activities. For instance, on-road transportation scaling factors exhibited 2 peaks with a scaling factor of about 1.3 at 7:00 and 1.8 at 17:00. These peaks represent increased transportation activity associated with the typical work day. This scaling factor dropped to 0.2 during the evening hours after the work day had ended. The scaling factors for industry were much smoother indicating continuous production through the whole day. Further details regarding this diurnal scaling approach can be found in Hu et al. (2018).

Anthropogenic CO₂ emissions should also exhibit seasonal variations related to the interaction between human activities and the influence of different weather conditions. Here, we derived monthly scaling factors using Carbon Tracker statistics (Peters et al. 2007). For winter (October, January, and

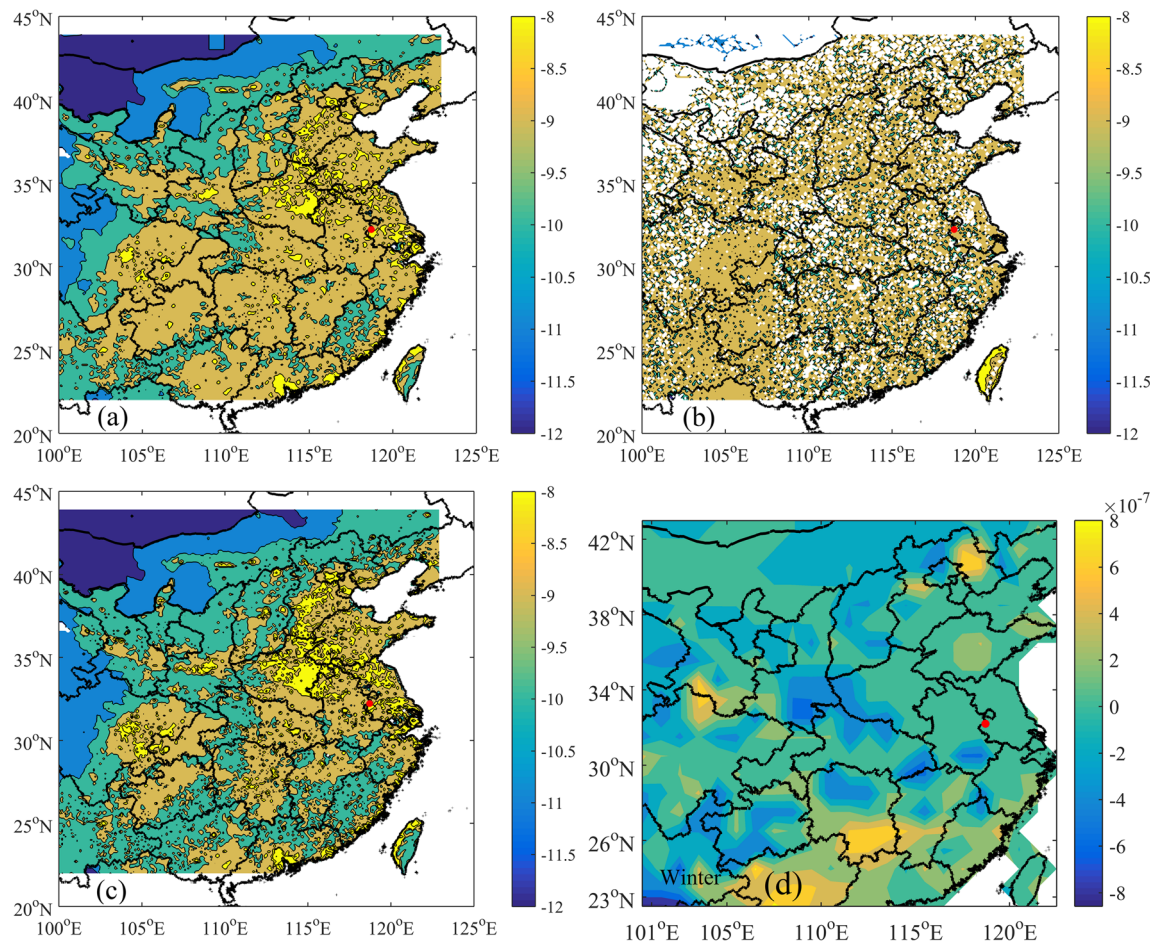


Fig. 2 Anthropogenic CO₂ emissions from different source categories including **a** residential, **b** on-road transportation, **c** combustion in

manufacturing industry, and **d** biological CO₂ flux in winter (unit mol m⁻² s⁻¹) for 2014

February), the scaling factors were adjusted higher to account for greater residential heating (Table 1). Here, the scaling factors were larger than 1 from October to March. The approach used here also accounts for regional differences associated with climate. For instance, the Yangtze River Delta area (domain1) has smaller monthly scaling factors than North China (contained by domain3) because North China is much colder than the Yangtze River Delta area. There is greater need, therefore, for more coal and natural gas burning during the heating season.

WRF-STILT model setup

Simulation of CO₂ mixing ratios

Following previous studies (Ahmadov et al. 2009; Mallia et al. 2015; Hu et al. 2018), the CO₂ mixing ratio was simulated as the sum of background ($CO_{2, bg}$), enhancements contributed by local sources of combustion ($\Delta CO_{2, comb}$), and biological CO₂ flux ($\Delta CO_{2, NEE}$) as described in eq. (1). Local anthropogenic combustion source contributions were divided

into fossil fuel use ($\Delta CO_{2, ff}$) and biomass burning ($\Delta CO_{2, bb}$) as described in eq. (2). Fossil fuel CO₂ fluxes were further separated into sub-categories. The contributions from different sources were modeled by multiplying each a priori CO₂ flux with the source footprint function as defined by eq. (3),

$$CO_{2,model} = CO_{2,bg} + \Delta CO_{2,comb} + \Delta CO_{2,NEE} \quad (1)$$

$$\Delta CO_{2,comb} = \Delta CO_{2,ff} + \Delta CO_{2,bb} \quad (2)$$

$$\Delta CO_2 = \sum_{i=1}^n \left[\left(foot_i \times (flux_{CO_2})_i \right) \right] \quad (3)$$

where ΔCO_2 is the modeled hourly CO₂ enhancement (contribution) from CO₂ sources (sinks), $flux_{CO_2}$ represents CO₂ emissions from different source or sink categories, $foot$ is the concentration source footprint simulated using the WRF-STILT model (Lin et al. 2003), and n is the integration time that contributes to each simulated hourly enhancement. Our previous work has shown that nearly 90% of the source contribution was determined by the past 24 h (Hu et al. 2018). Therefore, we set $n = 7$ days (168 h) to adequately account for the CO₂ enhancement; i is the corresponding hour over the 7-

Table 1 Monthly scaling factors applied for anthropogenic emissions for the study domains

	Jan	Feb	Mar	Apr	May	Jun	Jul	Aug	Sep	Oct	Nov	Dec
Domain 3	1.08	1.06	1.03	0.99	0.93	0.90	0.87	0.91	0.97	1.01	1.09	1.15
Domain 1	1.04	1.03	1.01	0.99	0.94	0.93	0.91	0.94	0.98	1.01	1.06	1.11

day period. In general, each simulated hourly CO₂ mixing ratio is the sum of the accumulated enhancement and background value over the past 7 days.

The Stochastic Time-Inverted Lagrangian Transport (STILT) model can simulate the source footprint function as the air flows over the study domain and arrives at the observation site. STILT simulates the turbulent diffusion and horizontal transportation by releasing a large number of particles from the receptor (34 m tower) and tracks them backward in time. The footprint defined here should be regarded as an influence weighting function that defines how each discretized surface grid cell contributes to the observation site (Gerbig et al. 2003; Lin et al. 2003). STILT has been shown to have a high accuracy and has been applied to many different scalars (Mallia et al. 2015; Chen et al. 2016; Bagley et al. 2017; Hu et al. 2018). The footprint function is calculated as,

$$\text{foot}\left(x_r, t_r | x_i, y_j, t_m\right) = \frac{m_{\text{air}}}{h\rho(x_i, y_j, t_m)} \frac{1}{N_{\text{tot}}} \sum_{p=1}^{N_{\text{tot}}} \Delta t_{p,i,j,k} \quad (4)$$

where foot represents the influence for each upstream location(x_i, y_j) at the time t_m to the receptor (x_r), h is the influence height above each location and is estimated here as as half of the modeled PBL height, ρ is the average air density below the influence height, m_{air} is the molar mass of dry air, and N_{tot} is total number of particles released. Following previous work $N_{\text{tot}} = 500$.

The CO₂ background mixing ratios were derived from the Carbon Tracker global CO₂ distributions, which were simulated by the TM5 transport model (Peters et al. 2007; Pillai et al. 2012). The meteorological fields from the WRF3.5 model were used to drive the STILT model (details in section “**WRF model setup and verifications**”). For each 7-day period, we traced the 3-D locations of all 500 particles in the global background CO₂ dataset and obtained the average CO₂ mixing ratio which represents the background mixing ratio for each hour (Peters et al. 2007; Karion et al. 2016; Chen et al. 2016).

WRF model setup and verifications

To obtain accurate meteorological simulations, we used the common setup of 3 domains with 2-way feedback among each domain. The spatial resolution for the outer to inner-most domain was 27, 9, and 3 km, respectively. As shown in Fig. 1, domain 1 contains most of Central and East China (105 × 111 grid cells), domain 2 focused on the East China Region

(154 × 148 cells), and domain 3 contains the Yangtze River Delta (253 × 223 cells). Initial and boundary meteorological conditions were specified using the NCEP FNL 1° × 1° data (<http://rda.ucar.edu/datasets/ds083.2>). The model configurations are displayed in Table 2. Here, we have applied the model configurations that were tested and verified by Hu et al. (2017) for the same study domains. This previous study evaluated the WRF model performance in simulating the variations of 2 m air temperature, wind speed, wind direction, and downward shortwave radiation for Nanjing city. The model results indicated a mean error (ME) of 0.21 °C, 1.22 m s⁻¹, -39.57°, and 0.29 W m⁻², respectively. The root mean square errors (RMSE) were 1.12 °C, 1.68 m s⁻¹, 76.36°, and 161.72 W m⁻², respectively. The corresponding correlations between the simulated and observed values were 0.95, 0.47, 0.58, and 0.89, respectively. Overall, the model performed reasonably well.

Because the domain setup and WRF-STILT model is computationally expensive, we restricted our footprint simulations to the year 2014. Further, the CO₂ mixing ratios during winter were used to constrain the CO₂ emissions. This strategy was adopted to avoid the uncertainty introduced when considering relatively large biological fluxes during the summer months (Peters et al. 2007). The biological CO₂ flux in winter is much smaller as compared with anthropogenic emissions in our Yangtze River Delta (Fig. 3d). Within the scope of YRD, most of them are below 1 mol m⁻² s⁻¹, even a little uptake was shown in the south of Anhui Province, while it will not have too much effect on our observation site and it will be discussed in Section “**Three-year CO₂ mixing ratio observations**”. Here, the modeled CO₂ enhancements for Dec, Jan, and Feb associated with biological contributions were 0.84, 0.41, and -0.71 μmol mol⁻¹, respectively. These biological enhancements were negligible compared to the anthropogenic contributions from fossil (i.e., typically > 30).

Constraining anthropogenic emissions

The Bayesian inversion methodology has been used to constrain emissions from a variety of sources (i.e., N₂O, CH₄, and CO₂) (McKain et al. 2012; Chen et al. 2016; Pillai et al. 2016). Here, we take a simplified inversion method to constrain the total anthropogenic CO₂ emissions. The observed CO₂ enhancement was used to constrain a priori CO₂ emissions. The CO₂ enhancement was estimated by subtracting the background values from the tower observations (section

Table 2 WRF3.5 physical schemes

Basic equations	Non-hydro model
Microphysics	WSM 3-class
Longwave radiation	Rapid radiative transfer model (RRTM)
Shortwave radiation	Dudhia scheme
Surface-layer	Monin-Obukhov similarity scheme
Land surface	Noah land surface model
Boundary layer	YSU scheme
Cumulus	Kain-Fritsch (new Eta) scheme (domain 1 and domain 2)

“Simulation of CO₂ mixing ratios”). To reduce the potential uncertainty of biological CO₂ flux contributions, we restricted our analyses to the non-growing season (December, January, and February) (Shen et al. 2014; Xu et al. 2017). This is based on the fact that observed CO₂ concentration was much similar

in different years, and the simulation of CO₂ concentration in winter for only 1 year is enough to constrain anthropogenic emissions. We consider at the monthly timescale that the bias between observed and modeled CO₂ enhancements is derived from the bias in the a priori CO₂ emissions. We then use the

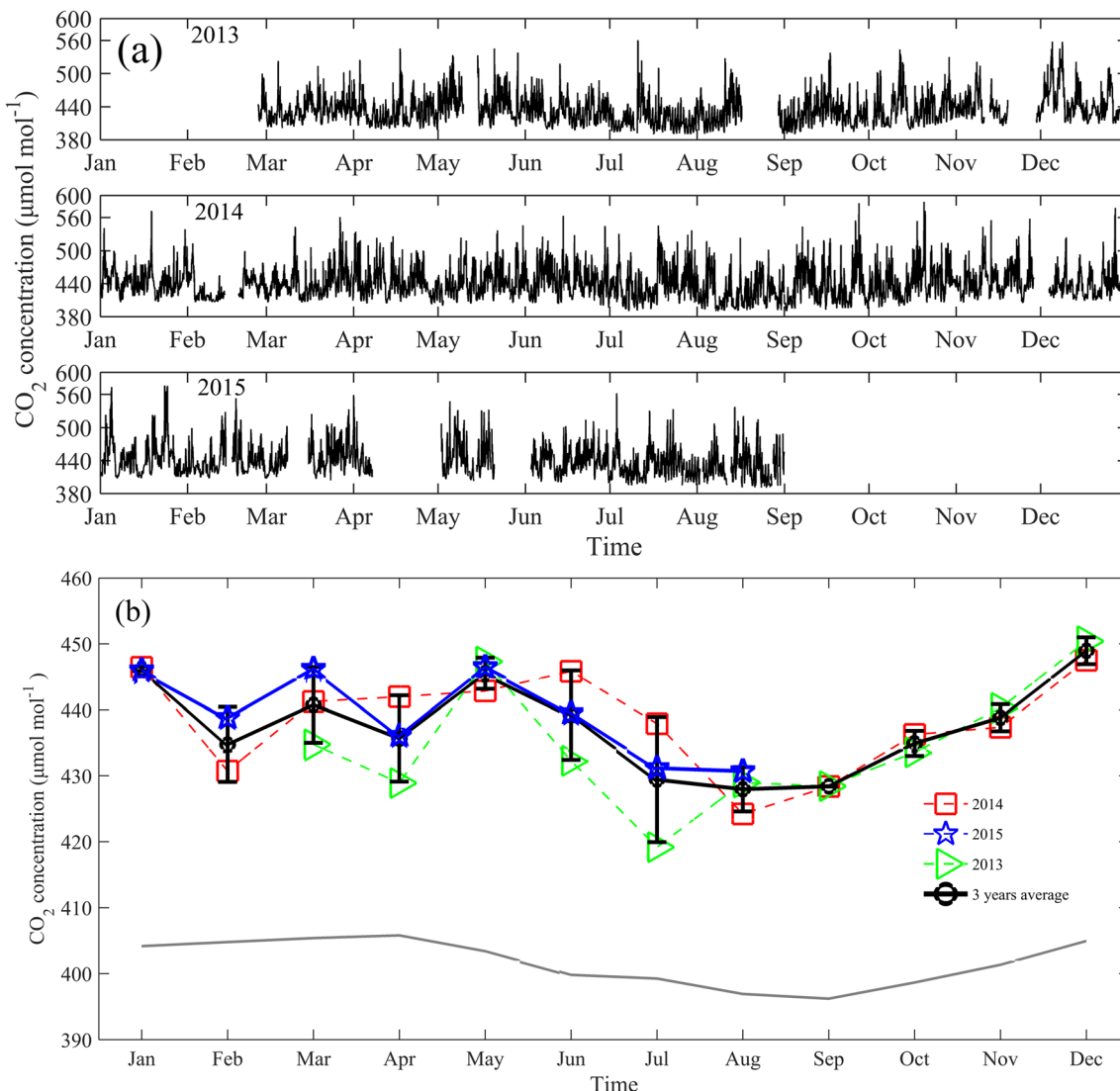


Fig. 3 **a** One hour aggregated time series of CO₂ mixing ratio from March 2013 to August 2015, and **b** monthly averaged concentration and its standard deviation through the observation period

enhancement ratio derived from the winter analysis to update the a priori emission map (Bray et al. 2017).

There are a number of uncertainties associated with our inversion methodology. The most important ones include bias in the a priori CO₂ emissions; errors in the background CO₂ data and observed mixing ratio; bias in the meteorological forcing data from WRF3.5, and the associated uncertainties in the back trajectories simulated by STILT. To account for the overall uncertainties, we take a Monte Carlo approach to assign uncertainty for each of the above factors (Brown et al. 2012; Shen et al. 2014). Here, we assign an uncertainty of 21% to the simulated PBL height from WRF3.5 following Chen et al. (2016); a 13% uncertainty was assigned to the STILT back trajectories (Gerbig et al. 2003; Miller et al. 2008; Chen et al. 2016; Chen et al., 2018). The uncertainty in the background CO₂ fields from Carbon Tracker's global CO₂ distributions was assigned a value of 2% based on previous study (Hu et al. 2018). Here, we assume normal distribution of each uncertainty with a mean value of 1. Using eq. 5, we performed the Monte Carlo simulation using 10,000 iterations to derive a total uncertainty for the inversion.

$$S_{\text{PBL}} \times S_{\text{particles}} \times S_{\text{background}} \times x \times R_{\text{enhancement_ratio}} = 1 \quad (5)$$

Where S_{PBL} , $S_{\text{particles}}$, and $S_{\text{background}}$ represent uncertainty in PBL, particles' numbers, and CO₂ background fields, respectively. X is the ratio between observed enhancement and modeled enhancement in the 3 months, and $R_{\text{enhancement_ratio}}$ is our derived scaling factors for the anthropogenic CO₂ emissions.

Results and discussion

Three-year CO₂ mixing ratio observations

The CO₂ mixing ratio observations from March 2013 to August 2015 are shown in Fig. 3a. These data indicate that there was very little seasonal variation among the 3 years. The short-term variations, however, were large and exceeded 100 μmol mol⁻¹. These large CO₂ variations were influenced by the direction of air flow and the influence of industrial zones. There was a strong interaction between meteorological conditions and surface CO₂ flux that caused pronounced changes in atmospheric CO₂ mixing ratios (Ahmadov et al. 2009; Guha and Ghosh 2010; Ballav et al. 2016). For instance, relatively shallow PBL depth and simultaneous large surface emissions cause atmospheric mixing ratios to exceed 500 μmol mol⁻¹. In 2014, CO₂ mixing ratios ranged from 390.0 to 560.7 μmol mol⁻¹, much smaller than the range (372.2 to 635.6) reported for Beijing in 2013 (Pang et al. 2016), where large coal combustion occurred during the heating seasons. Here, we focus our attention on the CO₂ enhancements, which can provide more insights regarding

the CO₂ contributions from local sources. The typical CO₂ enhancements in spring, summer, autumn, and winter were 23.52~49.65 μmol mol⁻¹, 21.36~52.37 μmol mol⁻¹, 28.14~55.41 μmol mol⁻¹, and 29.51~42.35 μmol mol⁻¹, respectively. These values were slightly higher than the summer observations reported for Salt Lake City, USA (i.e., 25 μmol mol⁻¹ in summer) (Pataki et al. 2003), and were nearly fourfold larger than values reported for Chicago (i.e., 7.3 μmol mol⁻¹ enhancement) during the summer (Moore and Jacobson 2015). The relatively high enhancement values in our observations reflect the large population density and associated fossil fuel consumption in the YRD.

To eliminate the short-term variations, we examined the monthly averaged CO₂ mixing ratios (Fig. 3b). Figure 3b indicates an important drawdown in CO₂ mixing ratios during the growing season (May–September) resulting from photosynthesis. Each year showed a similar influence of net ecosystem CO₂ exchange on the summertime CO₂ mixing ratios. Observations in winter will be used to constrain and evaluate anthropogenic CO₂ flux for the low CO₂ signals from plants' respiration. Interestingly, the observed CO₂ mixing ratios in February were much lower than in the previous January (11.5 μmol mol⁻¹) and following March (5.9 μmol mol⁻¹). We hypothesize that this was caused by the relatively low CO₂ emissions associated with the traditional Chinese New Year holiday. However, our model results indicated similarly low CO₂ mixing ratios in February despite having the same a priori emissions as observed in other months (see details in section “Comparing modeled versus observed CO₂ mixing ratios”). Therefore, the relatively low CO₂ mixing ratios observed in February appear to be related to the atmospheric circulation.

Variations of concentration footprint and cumulative CO₂ mixing ratio enhancement

To help understand the source areas that contribute to the observation site, we examined the cumulative CO₂ enhancement and its proportional change with time (Fig. 4). The total CO₂ enhancements in December, January, and February exhibited large differences with December values (35.9 μmol mol⁻¹) > January values (29.2 μmol mol⁻¹) > February values (25.0 μmol mol⁻¹). These model results were consistent with the CO₂ mixing ratio observations (Fig. 4b). Taking into account the difference in anthropogenic CO₂ emissions used for different months are within 10%, it indicated meteorological conditions lead to this large difference, and our model configuration can well model the PBL characters in different months.

Nearly 85% of the CO₂ enhancement was accumulated within a period of 24 h (Fig. 4b). Given a measured average wind speed of 10 m s⁻¹, we estimated that the source area that contributed 85% to the measured CO₂ enhancements was within a radius of about 1000 km. This indicates our observations are representative of the broader YRD region. We also

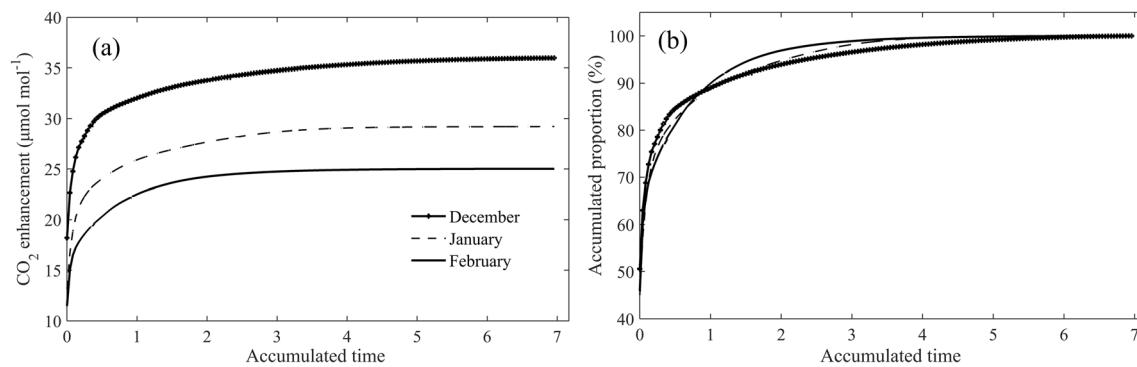


Fig. 4 Time series of accumulated CO₂ enhancement and its proportional change over the past 7 days

note that compared with other part in YRD, the Nanjing municipality should have much high influence weight. Our results were similar with the definition in Shen et al. (2014), who applied the CO₂ concentration at 34 m height to represent YRD in daytime and Nanjing in the nighttime considering the difference of boundary layer structures.

The source footprint functions were averaged on monthly timescales (Fig. 5) to help understand how variations in climate influence the tower observations. The annual average footprint (Fig. 5e) was more uniform for all directions than the monthly average. The northeastern monsoon in winter played an important role in changing the pattern of the footprint function giving it a strong northwest-southeast influence. Hu et al. (2011) and Chen et al. (2016) defined the most sensitive area contributing to the observation site as log₁₀ (footprint) larger than -4 (footprint units ppm μmol⁻¹ m² s). Here, the most sensitive footprint distance contains the majority of YRD, the eastern Anhui province, and the western Jiangsu province. These results support that our observations obtained at the 34 m height are strongly influenced by anthropogenic CO₂ signals from within the broader YRD area.

Here, we combine the computed annual footprint function with the a priori anthropogenic CO₂ emissions to calculate the CO₂ enhancement at the observation site. We followed the study of Shen et al. (2014) and separated the whole day into daytime (daytime as 10:00~17:00) and nighttime (nighttime as 23:00~5:00) contributions (Table 3). This separation is important as the footprint function varies according to these different planetary boundary layer conditions. The source area during the daytime was much smaller than during nighttime with lgF < -3 (here, lgF refers to log₁₀ (footprint)). Therefore, anthropogenic CO₂ enhancements were associated with more local sources during the daytime and controlled by much stronger vertical turbulence. When choosing the source area with lgF > -2.5, its area varied between 5.1×10^3 km² and 12.5×10^3 km², which was close to Nanjing municipality (6.6×10^3 km²). Also, the source areas with lgF > -3.5 represented area between 1.5×10^6 km² and 1.7×10^6 km², close to YRD (1.1×10^6 km²). Gloor et al. (2001) and Chen et al. (2014) applied backward trajectory method to quantify atmospheric

CO₂ source areas for tall towers with 100~200 m height. Their footprint area estimates were about 10^6 km² and in close agreement with our findings. Based on different footprint criteria, the averaged anthropogenic CO₂ flux varied considerably. For instance, CO₂ emissions from oil production/refineries decreased rapidly as the source footprint function distance increased indicating that industrial complexes played an important role as local sources.

Comparing modeled versus observed CO₂ mixing ratios

Monthly mean diurnal variations between the observations and model simulations are compared for the winter period (Fig. 6). In general, the modeled results (denoted as Modeled_h in Fig. 6) are close to the observations and exhibit similar diurnal patterns. The model results were a little smaller than observations in the daytime, and on the contrary in nighttime. This pattern resulted mainly from diurnal variations of the CO₂ emissions used in the WRF-STILT model. Here, only on-road emissions have a large diurnal pattern (0.2–1.8), while the scaling factors for industrial emissions show little diurnal variation and also account for the majority of the regional emissions. We performed a sensitivity test by applying on-road diurnal patterns on industry emissions; situations improved a lot during the nighttime as shown in Fig. 6d (Modeled_s). As shown in Fig. 6a–c, the WRF-STILT model can capture most of the synoptic variability at higher temporal resolution and will miss some of synoptic variability in the nighttime. It may be caused by both the modeling of synoptic scale systems and abrupt change of CO₂ emissions that cannot be reflected by CO₂ emission maps. Also, the model ability in simulating the PBL height can directly affect the simulation of CO₂ mixing ratios. Previous study indicated the simulated PBL height in nighttime may have larger uncertainty than in daytime, and lower simulation of PBL height can lead to higher CO₂ concentration, and vice versa (Bagley et al. 2017). Given the lack of direct PBL height observations, we cannot quantify the extent to which a bias would impact our results. Fu et al. (2017) compared modeled and observed PBL

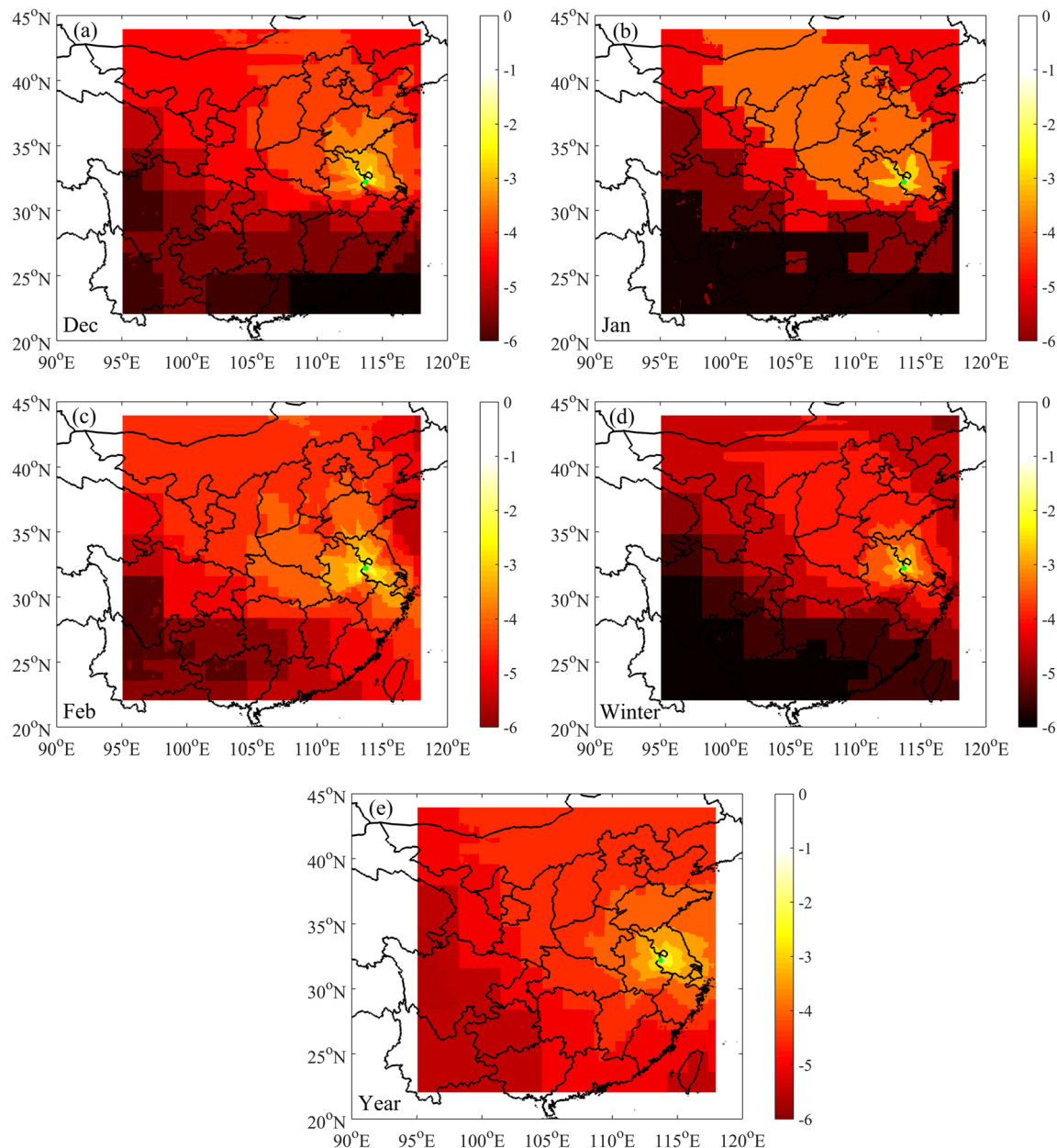


Fig. 5 Averaged footprint for **a** December, **b** January, **c** February, **d** Winter, and **e** the whole year (units \log_{10} ($\text{ppm } \mu\text{mol}^{-1} \text{ m}^2 \text{ s}$))

height with the similar domain configuration setup as ours but for Minneapolis, USA. They concluded that modeled PBL heights were in good agreement with PBL height observations.

The anthropogenic CO₂ enhancements have been shown to vary widely in the literature. Ahmadov et al. (2009) simulated the CO₂ enhancement contributed by fossil fuel at a coastal city site in France and found that the hourly contributions were within about $4 \mu\text{mol mol}^{-1}$ with monthly average values of about $1 \mu\text{mol mol}^{-1}$, which was caused by low anthropogenic activities and differed largely with the situation in Yangtze River Delta. Research conducted in Berlin,

Germany, also found much lower enhancement values of $6.3 \pm 2.9 \mu\text{mol mol}^{-1}$ than our results. While for the industrial city of Salt Lake City, USA, the anthropogenic CO₂ enhancement in the summer of 2007 and the maximum enhancements were larger than $30 \mu\text{mol mol}^{-1}$ (Mallia et al. 2015) and much closer to our findings. Hu et al. (2018) simulated 3 years CO₂ enhancement at an agricultural-urban landscape in Minneapolis-Saint Paul metropolitan, USA and concluded the annual CO₂ enhancement varied between 6.6 and $7.4 \mu\text{mol mol}^{-1}$. Most of the anthropogenic CO₂ enhancement was contributed by fossil combustion from industries.

Table 3 Averaged anthropogenic emissions based on footprint categories for daytime and nighttime in winter

Nighttime	[0, -1]	[-1.5, -1]	[-2, -1.5]	[-2.5, -2]	[-3, -2.5]	[-3.5, -3]	[-4, -3.5]
Area (100 km ²)	1	1	9	51	242	1467	5664
Manufacturing industry	14.49	9.82	5.77	6.48	4.91	5.61	2.73
Energy industry	0.00	0.00	16.47	18.00	8.85	5.63	4.78
Nonmetallic mineral processes	13.46	8.60	5.04	2.87	2.26	1.72	1.26
Oil production/refineries	97.42	47.05	10.15	2.94	0.95	0.53	0.38
Residential	3.83	2.60	1.69	1.12	0.99	0.75	0.64
Total anthropogenic emissions	132.83	70.86	40.86	33.13	19.26	15.50	10.59
Daytime							
Area (100 km ²)	1	9	40	125	437	1682	5097
Manufacturing industry	10.84	14.84	10.82	4.89	4.51	7.07	2.71
Energy industry	0.00	0.00	5.52	12.26	11.71	7.54	4.49
Nonmetallic mineral processes	10.07	13.79	9.57	4.23	2.27	2.09	1.24
Oil production/refineries	194.84	172.51	43.13	8.21	1.70	0.60	0.38
Residential	2.86	3.92	2.86	1.48	0.99	0.90	0.64
Total anthropogenic emissions	221.56	208.77	74.88	32.63	22.51	19.70	10.24

CO₂ sources and their influence on observed and modeled enhancements

Differences in the monthly averaged CO₂ enhancements between observations and model results are shown in Fig. 7. The results indicate a negative bias when using the a priori emissions from 2010 (S1). These a priori emissions do not include the changes that have occurred over the period 2010 to 2014. The ratio of 1.18

(recommended by EDGAR for all of China) was applied and is shown as S3 and obviously has a positive bias than observations (S3). Oil production (refinery) industries contributed the largest enhancement compared to other source categories., which represented the role of such industry in YRD's local CO₂ budget, and its proportions varied largely in these 3 months, indicating source areas changed controlled by meteorological conditions rather than emissions.

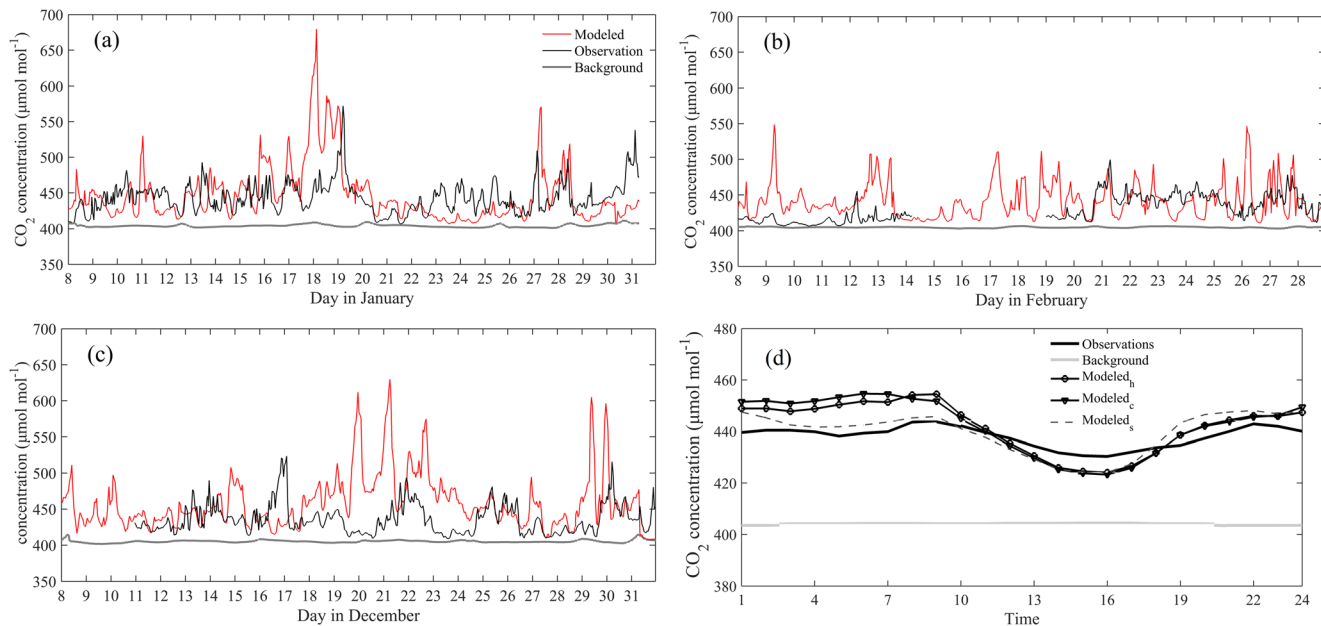


Fig. 6 Comparisons of observations and model results for **a** hourly CO₂ concentration in January, **b** February, **c** December, and **d** time averaged CO₂ mixing ratio diurnal variation between observations and modeled

results (Dec-Jan-Feb), Modeled_h, Modeled_c, Modeled_s represents hourly varied emissions, constant emissions, and intensive emissions

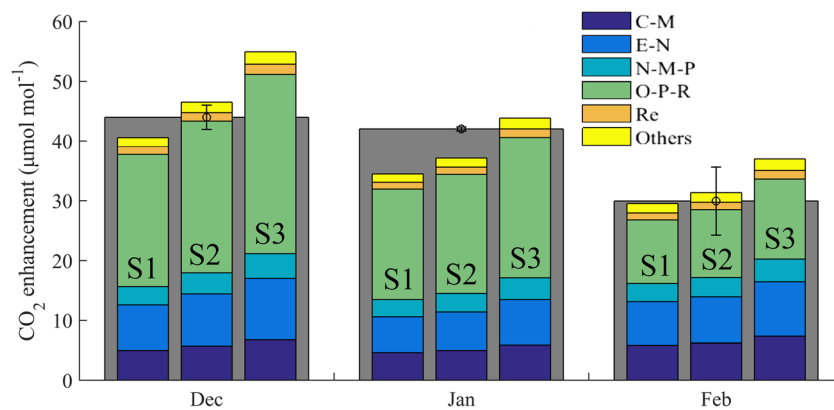


Fig. 7 Comparisons between monthly averaged observations and modeled results. Here, S1, S2, and S3 represent the modeled CO₂ enhancement by using constant emission map of 2010, monthly varied emission derived from the year of 2010, and emission map for 2014.

C-M, E-N, N-M-P, O-P-R, and Re represent the contribution from combustion in manufacturing industry, energy industry, nonmetallic mineral processes, oil production (refineries) industry, residential emission, and the rest anthropogenic categories, respectively

Monte Carlo simulations were performed to derive scaling factors based on the difference between observations and model results (methods described in section “[Constraining anthropogenic emissions](#)”). Here, we derived mean values of 0.91 and 0.25 for standard deviations from our Monte Carlo results. So, we concluded here that the anthropogenic CO₂ emission should be 0.162 (± 0.005) mg m⁻² s⁻¹, and it is $7 \pm 3\%$ higher than the emissions for 2010 for the Yangtze River Delta. Our results are in good agreement with Xu et al. (2017), who concluded that anthropogenic CO₂ emission was 0.17 (± 0.02) mg m⁻² s⁻¹ for YRD in 2014 based on IPCC method. Further, Shen et al. (2014) calculated the anthropogenic in YRD and reported a mean flux of 0.10 mg m⁻² s⁻¹ in 2009. According to the National Statistic Yearbook (Xu et al. 2017), the large observed increase of anthropogenic CO₂ emissions can be explained by the fact that the GDP has increased by 56% since 2009. Our findings and conclusions indicate high potential in anthropogenic CO₂ retrievals based on the inversion methodology described here. We note here that our results are based on the assumption that anthropogenic emissions have the same biases at local and regional scales and that uncertainty may exist given the potential for strong “aggregation error” (Zhao et al. 2009; Turner and Jacob 2015). Given the development of a greenhouse gas monitoring network for the greater YRD area, the new observations and inverse modeling should allow us to reduce the uncertainties in the anthropogenic CO₂ emission estimates. In this study, we have not evaluated the extent to which uncertainty in the PBL height can impact our results. In future work, we will make use of radiosonde data to evaluate these uncertainties.

Acknowledgements We would like to express our sincere thanks to Professor Timothy J. Griffis and Professor Xuhui Lee for advice in improving this paper’s logical organization and language, and also thank Professor R. Nassar for providing the hourly scaling factors for the different anthropogenic CO₂ source categories. The tall tower data

can be accessed at our group website (<https://yncenter.sites.yale.edu/zh-hans/data-access>).

Funding information This research was supported by National Natural Science Foundation of China (grants 41505005 and 41475141), the U.S. National Science Foundation (grants 1640337 and ATM-0546476), the Startup Foundation for Introducing Talent of Nanjing University of Information Science and Technology (grant no. 2014r046), the Natural Science Foundation of Jiangsu Province, China (grant BK20150900), the Ministry of Education of China under grant PCSIRT, and the Priority Academic Program Development of Jiangsu Higher Education Institutions.

References

- Ahmadv R, Gerbig C, Kretschmer R, Rner SK, Denbeck CR, Bousquet P et al (2009) Comparing high resolution WRF-VPRM simulations and two global co2 transport models with coastal tower measurements of CO₂. Biogeosciences 6(5):807–817
- Ballav S, Patra PK, Sawa Y, Matsueda H, Adachi A, Onogi S et al (2016) Simulation of CO₂ concentrations at tsukuba tall tower using wrf-co₂, tracer transport model. J Earth Syst Sci 125(1):47–64
- Bagley JE, Jeong S, Cui X, Newman S, Zhang J, Priest C, Campos-Pineda M, Andrews AE, Bianco L, Lloyd M, Lareau N, Clements C, Fischer ML (2017) Assessment of an atmospheric transport model for annual inverse estimates of California greenhouse gas emissions. J Geophys Res Atmos 122(3):1901–1918
- Bray CD, Battye W, Aneja VP, Tong D, Lee P, Tang Y, Nowak JB (2017) Evaluating ammonia (NH₃) predictions in the NOAA National Air Quality Forecast Capability (NAQFC) using in-situ aircraft and satellite measurements from the CalNex2010 campaign. Atmos Environ 163:65–76
- Brown K, et al. (2012) UK Greenhouse Gas Inventory, 1990 to 2010: annual report for submission under the framework convention on climate change. Didcot, AEA Technology, 357 pp.
- Bréon FM, Broquet G, Puygrenier V, Chevallier F, Xuerefrém I, Ramonet M et al (2015) An attempt at estimating paris area CO₂ emissions from atmospheric concentration measurements. Atmos Chem Phys 14(7):1707–1724
- Canadell JG, Ciais P, Dhakal S, Han D, Friedlingstein P, Gurney KR et al (2010) Interactions of the carbon cycle, human activity, and the climate system: a research portfolio. Curr Opin Environ Sustain 2(4):301–311

- Chen B, Zhang H, Coops NC, Fu D, Worthy DEJ, Xu G et al (2014) Assessing scalar concentration footprint climatology and land surface impacts on tall-tower co 2, concentration measurements in the boreal forest of central Saskatchewan, Canada. *Theor Appl Climatol* 118(1–2):115–132
- Chen Z, Griffis TJ, Millet DB, Wood J, Lee X, Baker JM et al (2016) Partitioning N₂O emissions within the US corn belt using an inverse modeling approach. *Glob Biogeochem Cycles* 30:1192–1205
- Chen Z, Griffis TJ, Baker JM, Millet DB, Wood JD, Dlugokencky EJ, Andrews AE, Sweeney C, Hu C, Kolkka RK (2018) Source partitioning of methane emissions and its seasonality in the U.S. Midwest. *J Geophys Res Biogeosci* 123:646–659
- European Commission (2009) Joint Research Centre/Netherlands Environmental Assessment Agency, Emission Database for Global Atmospheric Research (EDGAR), release version 4.0. European Environment Agency (EEA), Denmark
- Fu C, Lee X, Griffis TJ, Dlugokencky EJ, Andrews AE (2017) Investigation of the N₂O emission strength in the U.S Corn Belt. *Atmos Res* 194:66–77
- Gerbig C, Lin JC, Wofsy SC, Daube BC, Andrews AE, & Stephens BB, et al. (2003) Toward constraining regional-scale fluxes of CO₂ with atmospheric observations over a continent: 1. observed spatial variability from airborne platforms. *J Geophys Res Atmos* 108(D24), –
- Gloor M, Bakwin P, Hurst D, Lock L, Draxler R, Tans P (2001) What is the concentration footprint of a tall tower? *J Geophys Res* 106(D16): 17831–17840. <https://doi.org/10.1029/2001JD900021>
- Guha T, Ghosh P (2010) Diurnal variation of atmospheric CO₂, concentration and δ¹³C in an urban atmosphere during winter—role of the nocturnal boundary layer. *J Atmos Chem* 65(1):1–12
- Gurney KR, Mendoza DL, Zhou Y, Fischer ML, Miller CC, Geethakumar S, de la Rue du Can S (2009) The vulcan project: high resolution fossil fuel combustion CO₂ emissions fluxes for the United States. *Environ Sci Technol* 43(14):5535–5541
- Hu C, Liu SD, Cao C et al (2017) Simulation of atmospheric CO₂ concentration and source apportionment analysis in Nanjing City. *Acta Sci Circumst* 37(10):3862–3875 (in Chinese)
- Hu C, Griffis TJ, Lee X, Millet DB, Chen Z, Baker JM, Xiao K (2018) Top-down constraint on anthropogenic CO₂ emissions within an agricultural-urban landscape. *J Geophys Res Atmos.* <https://doi.org/10.1029/2017JD027881>
- Hu L, Millet DB, Mohr MJ, Wells KC, Griffis TJ, Helming D (2011) Sources and seasonality of atmospheric methanol based on tall tower measurements in the US Upper Midwest. *Atmos Chem Phys* 11(21): 17473–17505
- IPCC (2013) Climate change 2013: the physical science basis, IPCC Contribution of Working Group I to the Fifth Assessment Report of the Intergovernmental Panel on Climate Change. Cambridge University Press, Cambridge
- Karion A, Sweeney C, Miller JB, Andrews AE, Commane R, Dinardo S et al (2016) Investigating alaskan methane and carbon dioxide fluxes using measurements from the carver tower. *Atmos Chem Phys* 16(8): 5383–5398
- Kort EA, Frankenberg C, Miller CE, Oda T (2012) Space-based observations of megacity carbon dioxide. *Geophys Res Lett* 39(17): 17806
- Kort EA, Angevine WM, Duren R, Miller CE (2013) Surface observations for monitoring urban fossil fuel CO₂, emissions: minimum site location requirements for the Los Angeles megacity. *J Geophys Res Atmos* 118(3):1577–1584
- Liu Z, Guan D, Wei W, Davis SJ, Ciais P, Bai J et al (2015) Reduced carbon emission estimates from fossil fuel combustion and cement production in china. *Nature* 524(7565):335
- Lin JC, Gerbig C, Wofsy SC, Andrews AE, Daube BC, Davis KJ et al (2003) A near-field tool for simulating the upstream influence of atmospheric observations: the stochastic time-inverted lagrangian transport (stilt) model. *J Geophys Res Atmos* 108(4493):1211–1222
- Mallia DV, Lin JC, Urbanski S, Ehleringer J, Nehrkorn T (2015) Impacts of upwind wildfire emissions on CO, CO₂, and PM2.5 concentrations in Salt Lake City, Utah. *J Geophys Res Atmos* 120(1):147–166
- Mckain K, Wofsy SC, Nehrkorn T, Eluszkiewicz J, Ehleringer JR, Stephens BB (2012) Assessment of ground-based atmospheric observations for verification of greenhouse gas emissions from an urban region. *Proc Natl Acad Sci U S A* 109(22):8423
- Moore J, Jacobson AD (2015) Seasonally varying contributions to urban CO₂ in the Chicago, Illinois, USA region: insights from a high-resolution CO₂ concentration and δ¹³C record. *Burlingt Mag* 3(1109):000052
- Miller SM, Matross DM, Andrews AE, Millet DB (2008) Sources of carbon monoxide and formaldehyde in North America determined from high-resolution atmospheric data. *Atmos Chem Phys* 8(24): 7673–7696
- Ogle SM, Davis K, Lauvau T, Schuh A, Cooley D, & West TO, et al. (2015) An approach for verifying biogenic greenhouse gas emissions inventories with atmospheric CO₂ concentration data. *Environ Res Lett*, 10(3)
- Pang J, Wen X, Sun X (2016) Mixing ratio and carbon isotopic composition investigation of atmospheric CO₂, in Beijing, China. *Sci Total Environ* 539(539):322–330. <https://doi.org/10.1016/j.scitotenv.2015.08.130>
- Pataki DE, Bowling DR, Ehleringer JR (2003) Seasonal cycle of carbon dioxide and its isotopic composition in an urban atmosphere: anthropogenic and biogenic effects. *J Geophys Res Atmos* 108(108): 3047–3049
- Peylin P, Law RM, Gurney KR, Chevallier F (2013) Global atmospheric carbon budget: results from an ensemble of atmospheric CO₂ inversions. *Biogeosciences* 10(3):6699–6720
- Peters W, Jacobson AR, Sweeney C, Andrews AE, Conway TJ, Masarie K, Miller JB, Bruhwiler LMP, Petron G, Hirsch AI, Worthy DEJ, van der Werf GR, Randerson JT, Wennberg PO, Krol MC, Tans PP (2007) An atmospheric perspective on north american carbon dioxide exchange: carbontracker. *Proc Natl Acad Sci U S A* 104(48): 18925–18930
- Pillai D, Gerbig C, Kretschmer R, Beck V, Karstens U, Neininger B, Heimann M (2012) Comparing Lagrangian and Eulerian models for CO₂ transport – a step towards Bayesian inverse modeling using WRF/STILT-VPRM. *Atmos Chem Phys* 12:8979–8991
- Pillai D, Buchwitz M, Gerbig C, Koch T, Reuter M, Bovensmann H et al (2016) Tracking city CO₂ emissions from space using a high-resolution inverse modelling approach: a case study for Berlin, Germany. *Atmos Chem Phys* 16(15):1–35
- Rosenzweig C, Solecki W, Hammer SA, Mehrotra S (2010) Cities lead the way in climate-change action. *Nature* 467(7318):909–911
- Rypdal K, Winiwarter W (2001) Uncertainties in greenhouse gas emission inventories—evaluation, comparability and implications. *Environ Sci Pol* 4(2–3):107–116
- Shen S, Yang D, Xiao W, Liu S, Lee X (2014) Constraining anthropogenic CH emissions in Nanjing and the Yangtze River Delta, China, using atmospheric CO and CH mixing ratios. *Adv Atmos Sci* 31(6): 1343–1352
- Sun Y, Frankenberg C, Wood JD et al (2017) OCO-2 advances photosynthesis observation from space via solar-induced chlorophyll fluorescence. *Science* 358(6360):eaam5747
- Satterthwaite D (2008) Cities' contribution to global warming: notes on the allocation of greenhouse gas emissions. *Environ Urban* 20(2): 539–550
- Stauffer J, Broquet G, Bréon FM et al (2016) The first 1-year-long estimate of the Paris region fossil fuel CO₂ emissions based on atmospheric inversion. *Atmos Chem Phys* 16(22):1–34

- Turner AJ, Shusterman AA, McDonald BC, Teige V, Harley RA, Cohen RC (2016) Network design for quantifying urban CO₂ emissions: assessing trade-offs between precision and network density. *Atmos Chem Phys*, 16 (21):1–20
- Turner AJ, Jacob DJ (2015) Balancing aggregation and smoothing errors in inverse models. *Atmos Chem Phys* 15(1):1001–1026
- Turnbull JC, Sweeney C, Karion A, Newberger T, Lehman SJ, Tans PP et al (2015) Toward quantification and source sector identification of fossil fuel CO₂ emissions from an urban area: results from the influx experiment. *J Geophys Res Atmos* 120(1, 292):–312
- Wang R, Tao S, Ciais P, Shen HZ, Huang Y, Chen H, Shen GF, Wang B, Li W, Zhang YY, Lu Y, Zhu D, Chen YC, Liu XP, Wang WT, Wang XL, Liu WX, Li BG, Piao SL (2013) High-resolution mapping of combustion processes and implications for CO₂ emissions. *Atmos Chem Phys* 13(10):5189–5203
- Xu J, Lee X, Xiao W et al (2017) Interpreting the 13C/12C ratio of carbon dioxide in an urban airshed in the Yangtze River Delta, China. *Atmos Chem Phys* 17(5):3385–3399
- Zhao Y, Nielsen CP, McElroy MB (2012) China's CO₂ emissions estimated from the bottom up: recent trends, spatial distributions, and quantification of uncertainties. *Atmos Environ* 59:214–223
- Zhao C, Andrews AE, Bianco L, Eluszkiewicz J, Hirsch A, Macdonald C et al (2009) Atmospheric inverse estimates of methane emissions from Central California. *J Geophys Res Atmos* 114(D16):4723–4734